Supplementary Information (SI) for ChemComm.
This journal is © The Royal Society of Chemistry 2026

Electronic Supplementary Information

Plasmon-Enhanced Fluorescent Nanoprobe for Ultrasensitive and Selective Detection of Nitroaniline Derivatives

Farhin Akhtar[a, ǂ], Santanu Dolai[b, ǂ], Sabyasachi Pramanik[a,*], Satyapriya Bhandari[c,*]

[a]Department of Engineering Sciences, Rajiv Gandhi Institute of Petroleum Technology Sivasagar Campus, Sivasagar, Assam–785697, India
[b]Department of Chemistry, Indian Institute of Technology Guwahati, Assam–781039, India.
[c]Department of Chemistry, Kandi Raj College, Affiliated to University of Kalyani, West Bengal-742137, India

**** Corresponding Author E-mails:** satyapriya.bhandari@krc.edu.in; spramanik@rgipt.ac.in*

ǂ Authors contributed equally.

Experimental Section

A. Chemicals

All reagents were of analytical grade and used as received without further purification. Silver nitrate ($AgNO_3$) was obtained from SRL, while sodium borohydride ($NaBH_4$), 8-hydroxyquinoline-5-sulfonic acid (HQS), zinc acetate dihydrate (≥99%), methanol, and hydrochloric acid (HCl) were purchased from Merck. Nitroaromatic compounds—2,4-dinitroaniline (2,4-DNA), 4-nitroaniline (4-NA), 2,4-dinitrotoluene (2,4-DNT), 2,6-dinitrotoluene (2,6-DNT), 4-nitrotoluene (4-NT), 4-nitrobenzene (4-NB), and 4-nitrophenol (4-NP)—as well as aniline, ethylenediamine (EDA), and tetraethylamine (TEA) were also procured from Merck. Metal salts including $CaCl_2$, $CuCl_2$, $FeCl_3$, KCl, $NiCl_2$, $MgCl_2$, and NaCl were used for selectivity and interference studies. Deionized water (resistivity ≥18 MΩ·cm) was used throughout all experiments.

B. Synthesis of HQS-Stabilized Silver Nanoparticles (HQS-AgNPs)

HQS-stabilized silver nanoparticles were synthesized using a modified chemical reduction method. In a typical synthesis, 10.0 mM HQS aqueous solution was mixed with freshly prepared 20.0 mM $NaBH_4$ solution under continuous stirring in an ice-cold environment to ensure controlled nucleation. Subsequently, 10 mM $AgNO_3$ solution was added dropwise to the reaction mixture (total volume 40.0 mL) within 1 min. The appearance of a brown color indicated the formation of AgNPs. The resulting dispersion was purified by overnight dialysis against deionized water using a pre-cleaned dialysis membrane (MWCO 3.5 kDa) to remove excess ions and byproducts. The obtained colloidal HQS-AgNPs were stored at 4 °C for further characterization and nanoprobe fabrication.[S1]

C. Synthesis of Plasmon-Enhanced Fluorescent Nanoprobe (PEFN: Zn–HQS–AgNPs)

The plasmon-enhanced fluorescent nanoprobe (PEFN) was fabricated by introducing zinc acetate solution into the HQS-AgNP dispersion. A 0.1 mM zinc acetate dihydrate solution was added dropwise to the HQS-AgNP dispersion (absorbance ≈ 0.14 at 402 nm) under gentle stirring at room temperature. Optimization via fluorescence titration (Figure S1, Supporting Information) determined the ideal Zn^{2+} concentration to be 1.5 μM in a 3.0 mL AgNP dispersion, corresponding to maximum emission enhancement and stoichiometric balance. The synthesized PEFN sample exhibited pH ~ 6.8 and the nanocomposite was used directly for sensing experiments and stability analyses.

D. Sensing of 2,4-Dinitroaniline (2,4-DNA) and 4-Nitroaniline (4-NA)

The sensing capability of the PEFN (originally synthesized at pH 6.8) toward nitroaniline-based analytes was evaluated fluorometrically. Incremental additions of 0.1 mM of 2,4-DNA and 4-NA stock solutions were made to 3.0 mL of PEFN dispersion (absorbance ≈ 0.16 at 375 nm). After each addition, fluorescence spectra were recorded using an excitation wavelength of 365 nm. Each measurement was performed in triplicate, and the quenching efficiency was analyzed using the Stern–Volmer relationship. The limit of detection (LOD) was calculated using the equation $LOD = 3\sigma/k$, where σ is the standard deviation of the blank and k is the slope of the calibration plot (Figure 2A-2B-2C). The maximum amount of 4NA and 2,4 DNA added PEFN exhibited pH as ~ 6.94 and ~ 6.95, respectively.

E. Selectivity and Interference Studies

Selectivity experiments were performed to evaluate the specificity of the PEFN toward 2,4-DNA and 4-NA in the presence of potentially interfering species. Organic molecules (2,4-DNT, 2,6-DNT, 4-NT, 4-NB, 4-NP, aniline, EDA, and TEA) and various metal ions (Ca^{2+}, Cu^{2+}, Fe^{3+}, K^{+}, Ni^{2+}, Mg^{2+}, and Na^{+}) were each tested at a final concentration of 15 μM, which is at least 2.5 times higher than the analyte concentration. The fluorescence responses were recorded (Figure 2D-2E) to assess cross-reactivity. The results revealed a negligible response from the interferents, confirming the high selectivity of the PEFN toward the target nitroanilines.

F. Real-Sample Analysis

To validate the practical applicability of the PEFN, real-water samples (tap and river water) were analyzed. The samples were filtered through Whatman No. 42 paper followed by a 0.2 µm syringe filter to remove particulates. Spiked solutions containing 0.208 µM of 2,4-DNA or 4-NA were prepared in 3.0 mL of PEFN dispersion, and fluorescence intensities were measured. Analyte concentrations were quantified using calibration plots obtained from laboratory standards (Figure 2). Recovery percentages and relative standard deviations (RSD, n = 3) are summarized in Table 1, confirming the robustness and accuracy of the nanoprobe in complex matrices.

G. Characterization and Instrumentation

All optical measurements were carried out at room temperature. UV–Vis absorption spectra were recorded using a PerkinElmer Lambda 35 UV–Vis spectrophotometer, and photoluminescence spectra were measured on a HORIBA Jobin Yvon FluoroMax-4 spectrofluorimeter. Thin-film XRD patterns were collected using a Rigaku TTRAX-III diffractometer (Cu Kα radiation, λ = 1.5406 Å). TEM and HRTEM images were obtained using a JEOL JEM-2100F microscope operated at 200 kV, and the micrographs were analyzed with Gatan Digital Micrograph software. FTIR spectra were acquired using a PerkinElmer Spectrum Two spectrometer with an ATR accessory. SEM images were captured using a Zeiss Sigma 300 microscope. Zeta potential measurements were performed using a Malvern Zetasizer Nano ZS to assess colloidal stability and surface charge (Figure S6). Fluorescence lifetime measurements were conducted on a HORIBA Jobin Yvon Ultima Ultrafast 01-DD spectrofluorometer to determine excited-state dynamics.

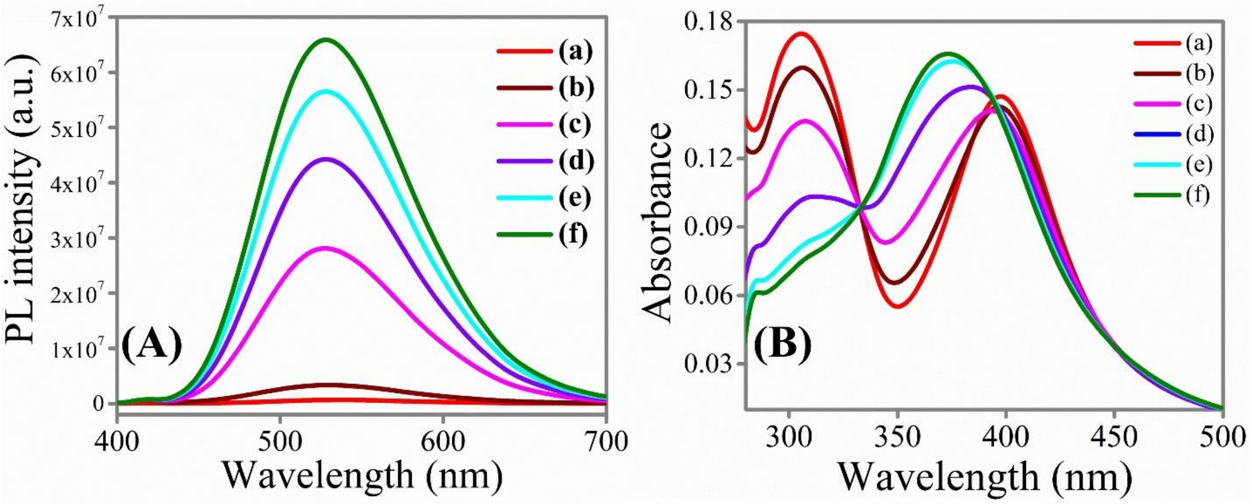

Fig. S1. (A) Fluorescence and **(B)** UV–Vis absorption titration profiles used to determine the optimal Zn^{2+} concentration [(a) 0.0; (b) 0.16;(c) 0.66; (d) 0.82; (e) 1.15; (f) 1.50 μM] for efficient coordination-driven assembly of PEFN. [S1-S3] Fluorescence and absorption titrations identify the optimal Zn^{2+} concentration for efficient coordination-driven assembly of the hybrid nanostructure.

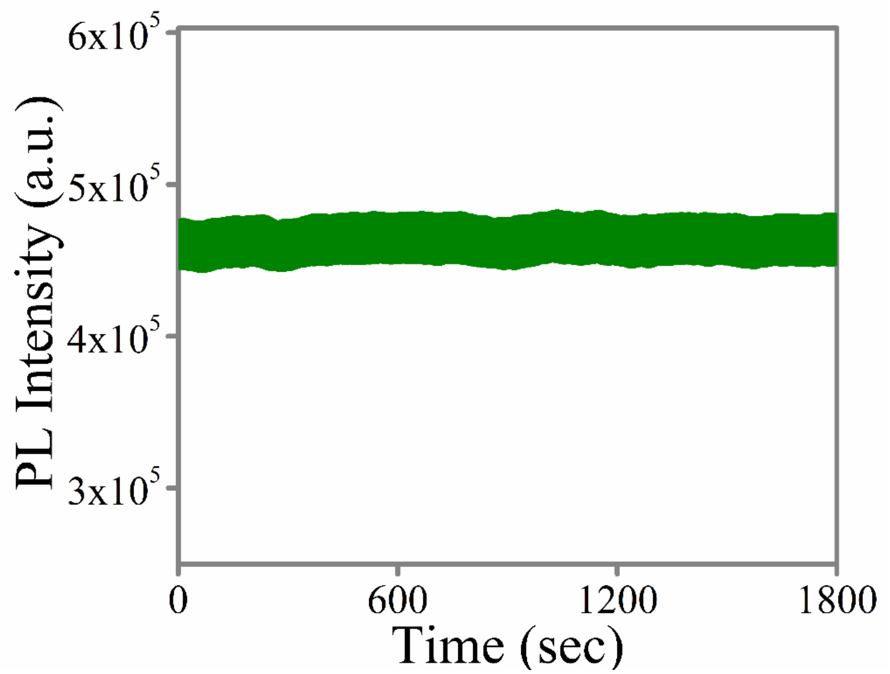

Fig. S2. Photostability of PEFN, demonstrating >95% emission retention after 30 min of continuous UV irradiation. The nanohybrid exhibited more than 95% of its initial emission intensity after 30 min of continuous UV light irradiation.

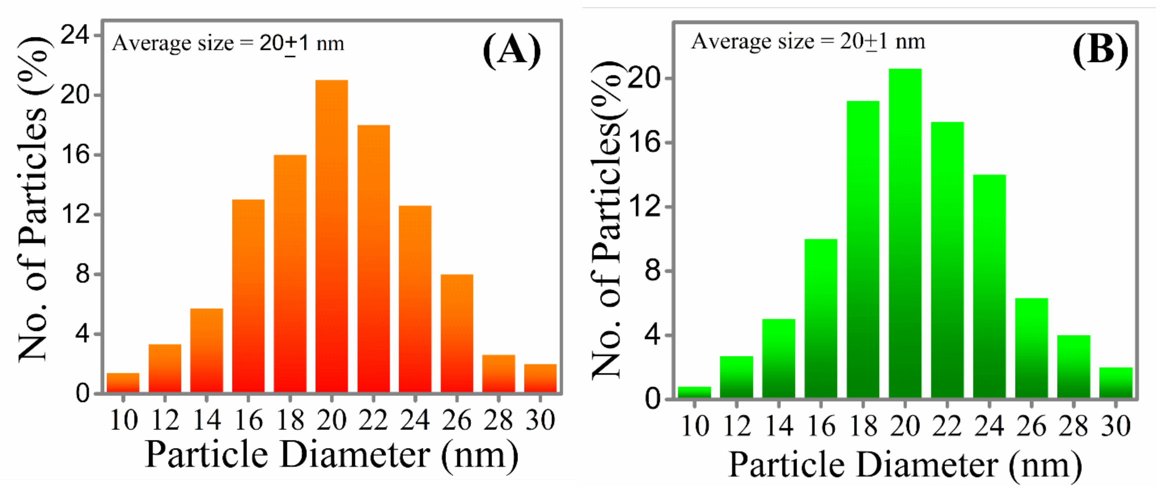

Fig. S3. Particle size distribution of **(A)** HQS-stabilized AgNPs and **(B)** PEFN, confirming uniform nanoscale morphology.

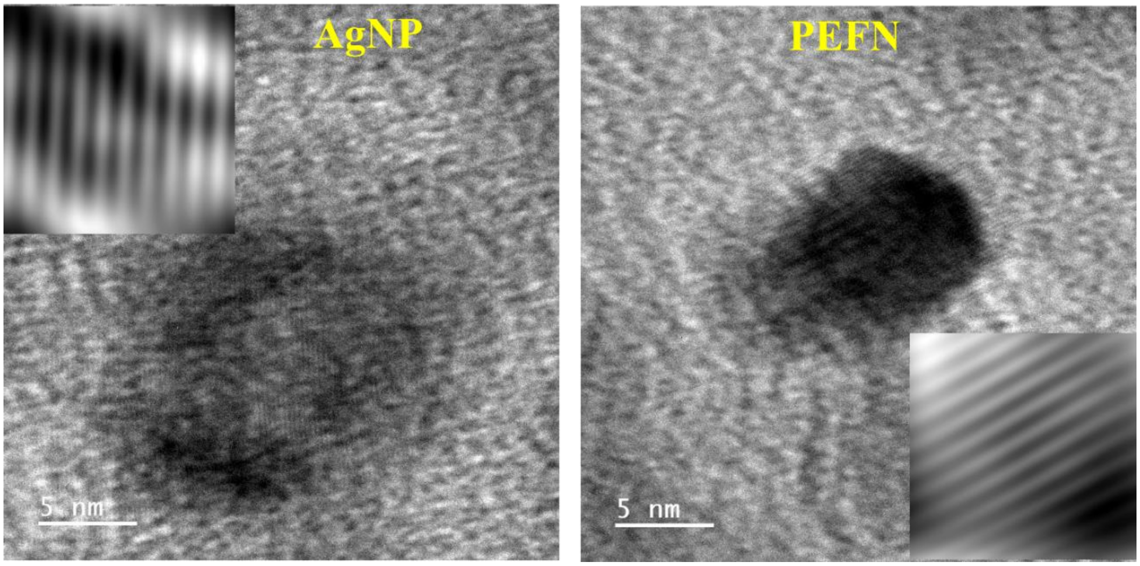

Fig. S4. HRTEM images of HQS-stabilized AgNPs and PEFN, both of having lattice spacing (d_{111}) 0.24 nm, illustrating structural integrity and successful composite formation.

Supporting particle size distribution and HRTEM images (**Fig. S3-S4, ESI**) showed narrow size distributions and well-resolved lattice fringes corresponding to the Ag (111) plane, demonstrating high crystallinity and uniform coordination-mediated assembly

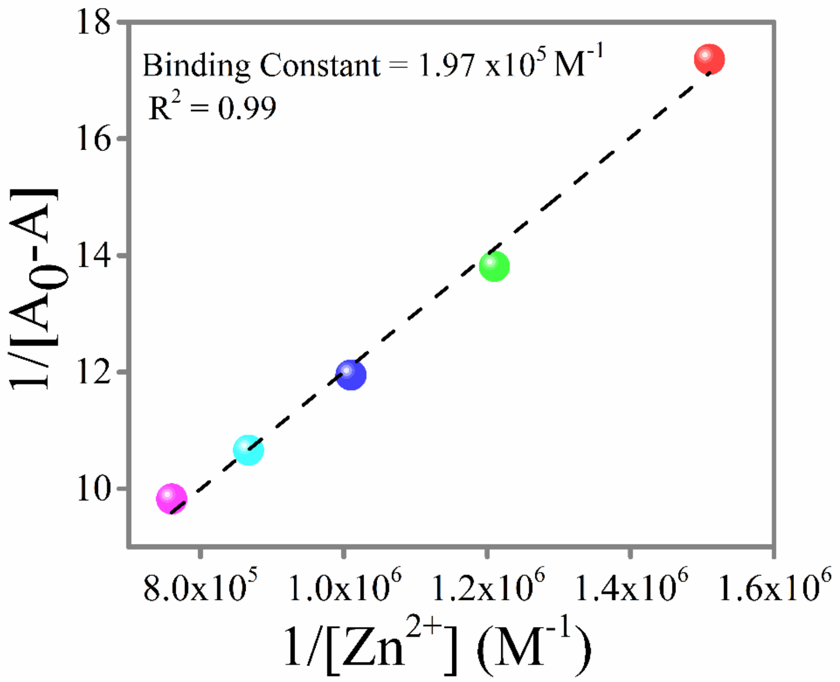

Fig. S5. Benesi–Hildebrand plot used to calculate the binding constant, indicating strong Zn^{2+} affinity for HQS–AgNPs and formation of a stable PEFN.[S4] Benesi–Hildebrand analysis gives a binding constant of 1.97 $\times 10^5$, indicating strong Zn^{2+} coordination with HQS-functionalized Ag NPs.

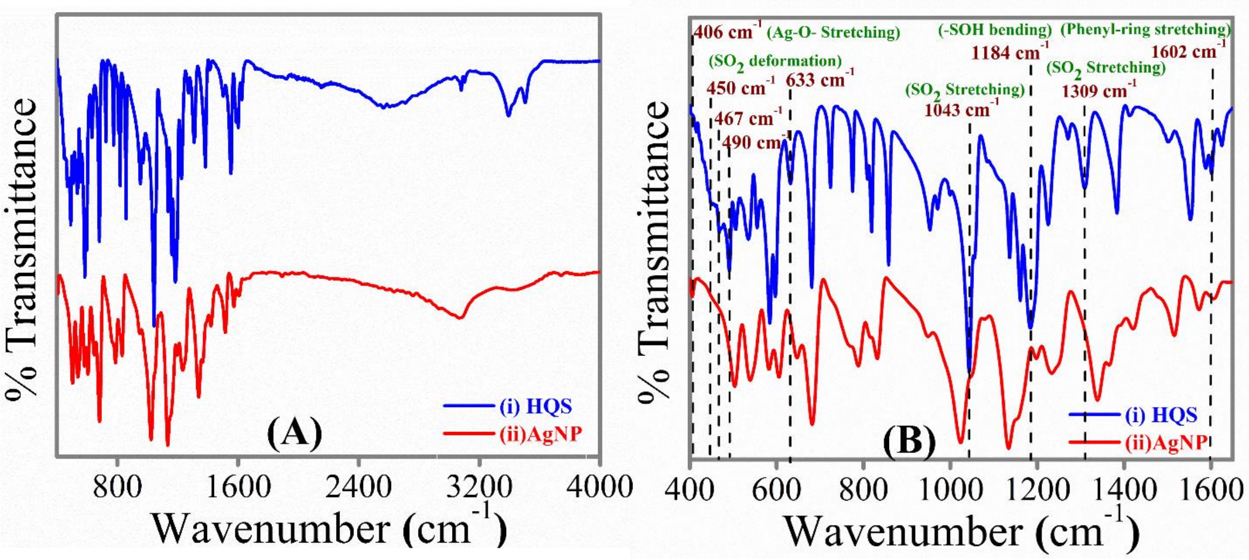

Fig. S6. **(A)** Full FTIR spectra (400–4000 cm^{-1}) and **(B)** expanded view (400–1600 cm^{-1}) of (i) HQS ligand and (ii) HQS-stabilized AgNPs and highlighting characteristic vibrational features.[S5-S6]

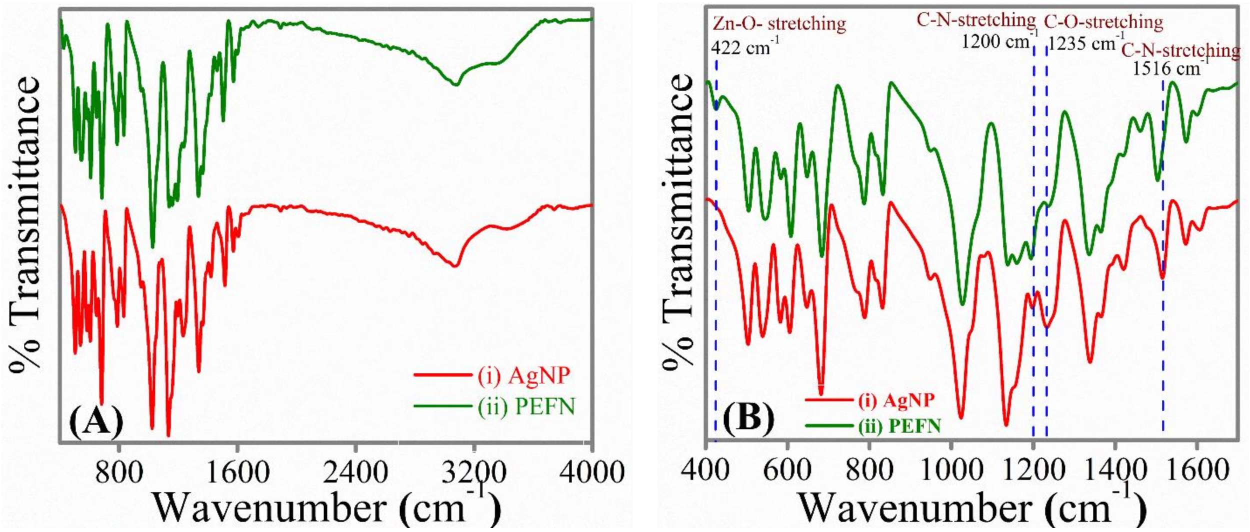

Fig. S7. (A) Full FTIR spectra (400–4000 cm^{-1}) and **(B)** expanded view (400–1600 cm^{-1}) of (i) HQS-stabilized Ag NPs and (ii) PEFN confirming ligand–nanoparticle interactions.[S7-S9]

FTIR Explanation: FTIR spectroscopy (Fig. S6–S7) provided molecular-level evidence for the coordination processes governing PEFN assembly. HQS-stabilized Ag NPs exhibited characteristic shifts in the sulfonate asymmetric and symmetric stretching bands (1200-1300 cm^{-1}), along with the appearance of an Ag-O coordination band at 406 cm^{-1} (Fig. S6, ESI).[S5-S6] Upon introduction of Zn^{2+}, the C=N (~1600 cm^{-1}) and O-H (~3300 cm^{-1}) vibrational modes shifted to lower wavenumbers, accompanied by the emergence of Zn-N/O stretching features near 422 cm^{-1}, confirming formation of the Zn-HQS coordination complex that promotes nanoparticle assembly (Fig. S7, ESI).[S7-S9]

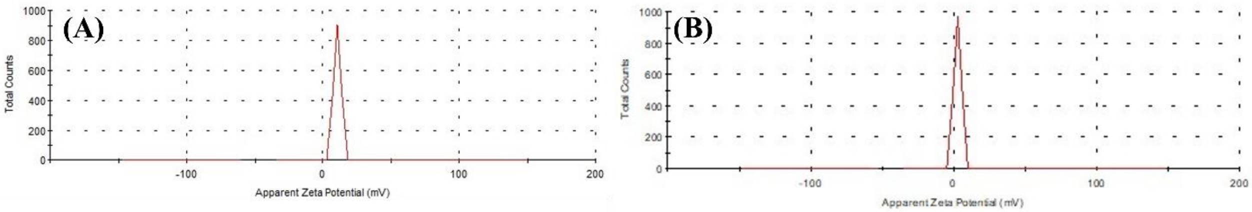

Fig. S8. Zeta-potential measurements of **(A)** AgNPs (−1.26 mV) and **(B)** PEFN (+0.29 mV), showing surface charge modification upon functionalization. Consistent zeta-potential changes (Fig. S8, Table S2, ESI) further verified systematic surface-charge modulation during hybrid formation.

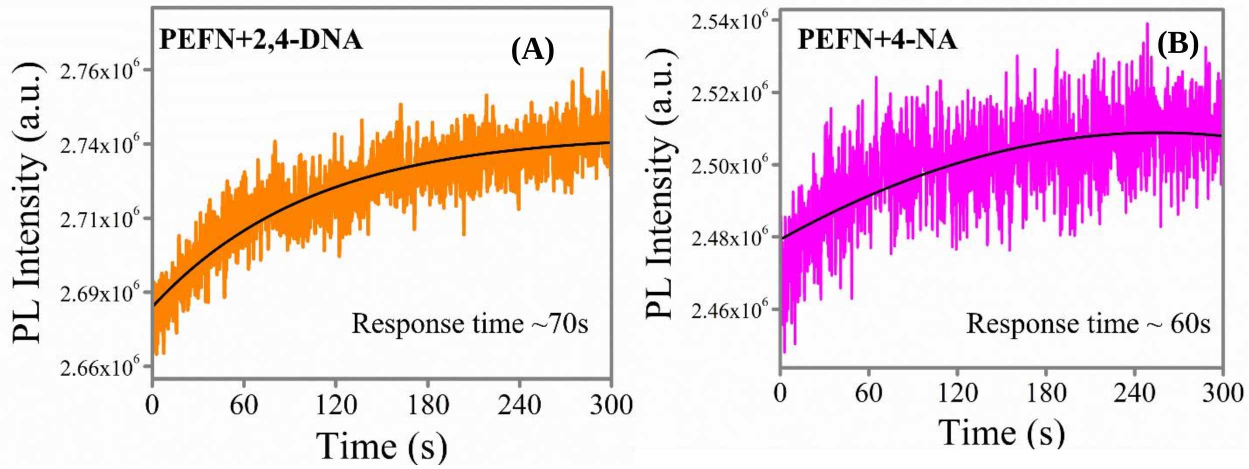

Fig. S9. Time-dependent fluorescence response of PEFN upon addition of nitroaniline (within the linear response range), showing that ~90% of the maximum signal change is achieved shortly after analyte (concentration of analyte used as 1.458 μM) addition, indicating rapid sensing.

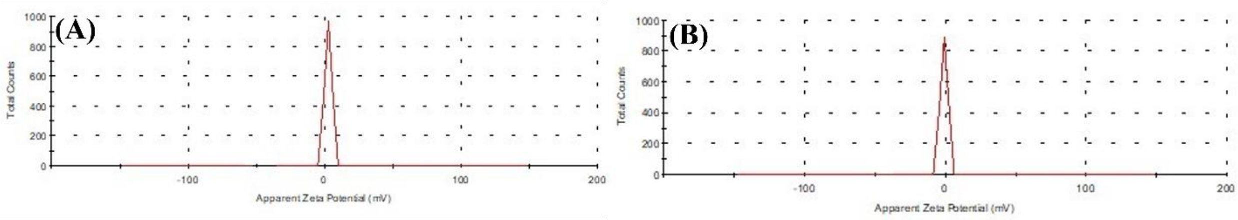

Fig. S10. Zeta-potential profiles of PEFN after interaction with **(A)** 2,4-DNA (-0.85mV) and **(B)** 4-NA (-0.44mV), showing a shift from +0.29 mV to slightly negative values, confirming surface coordination and charge reversal. Zeta-potential analysis (Fig. S8 and Fig. S10, ESI) provides compelling evidence for complexation: the initially weakly positive surface charge of PEFN (+0.29 mV) shifts to slightly negative values upon addition of the analytes, consistent with adsorption of nitro-rich, electron-withdrawing molecules that neutralize and subsequently invert the Zn^{2+}-dominated surface potential.

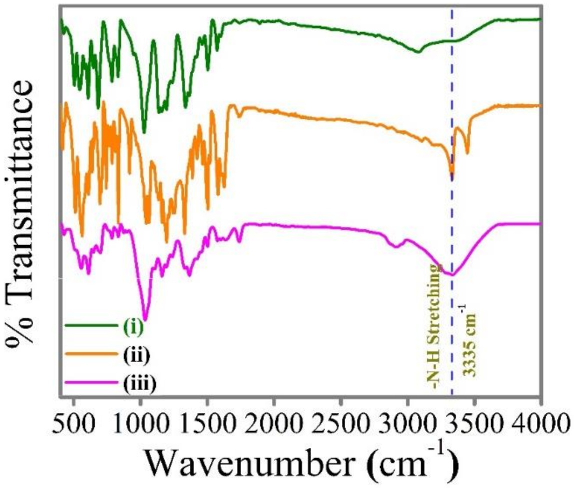

Fig. S11. FTIR spectra of PEFN in the **(i)** absence and presence of **(ii)** 2,4-DNA and **(iii)** 4-NA.

FTIR spectra (Fig. S10, ESI) show downshifts and broadening of the NH_2 stretching bands (3300–3500 cm^{-1}), confirming electron donation from the amine groups to Zn^{2+}.[29]

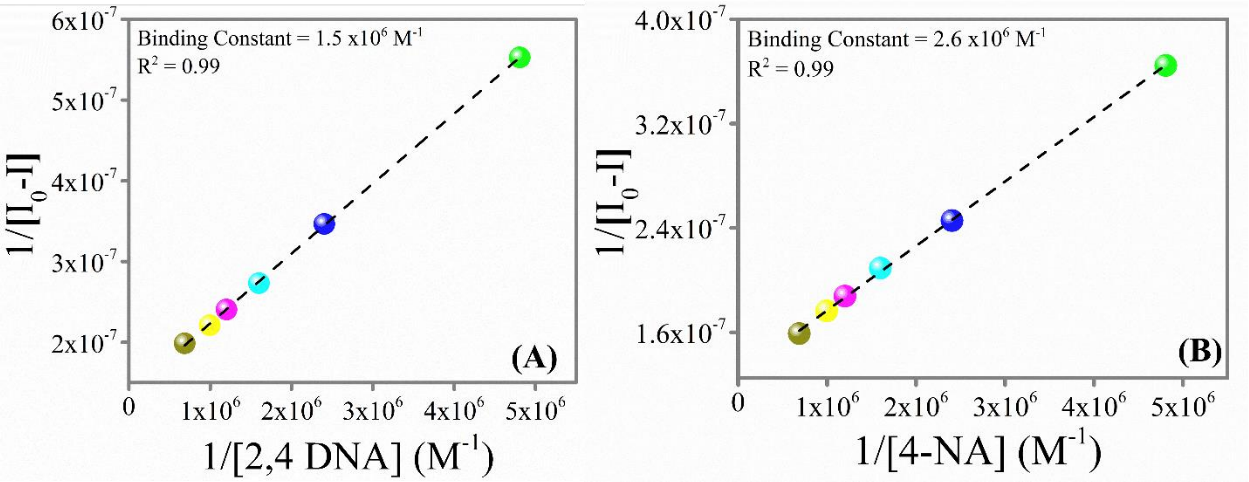

Fig. S12. Benesi–Hildebrand plot after addition of (A) 2,4-DNA and (B) 4-NA to PEFN composite. indicating strong binding affinity for the PEFN with nitro-aniline aromatic compound. The binding constant for 4-NA (2.6 × 10^6 M^{-1}) is substantially higher than that of 2,4-DNA (1.5 × 10^6 M^{-1}), clearly corroborating the stronger affinity of 4-NA toward PEFN (Fig. S11, ESI). This enhanced binding directly accounts for its lower LOD, compared to 2,4-DNA (Table S3, ESI). The reduced electron-donating capability of the -NH_2 group in 2,4-DNA - due to the presence of two strongly electron-withdrawing -NO_2 substituents - diminishes the efficiency of NH_2(NAD)→Zn^{2+}(PEFN) coordination. Consequently, its weaker ground-state complexation is reflected in its comparatively higher LOD, in agreement with the sensing results discussed earlier.

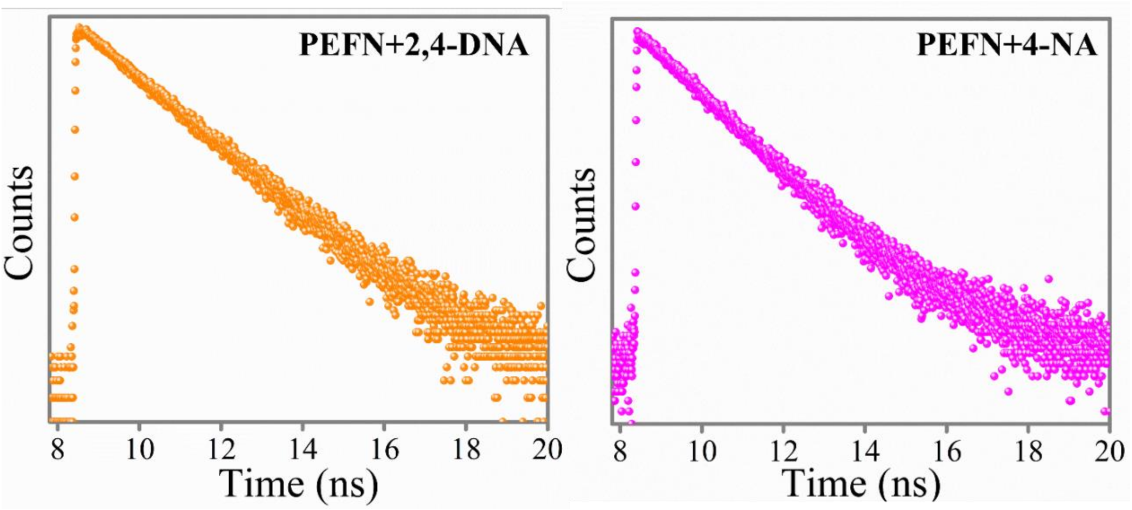

Fig. S13. Fluorescence lifetime decay profiles of PEFN after addition of 2,4-DNA and 4-NA, showing negligible changes in lifetime and confirming a static quenching mechanism. Fluorescence lifetime measurements reveal no significant change in decay profiles upon addition of either 4-NA or 2,4-DNA (Fig. S12, ESI), supporting a static rather than dynamic (collisional) quenching mechanism.[26,30] This further substantiates the formation of ground-state complexes between PEFN and the nitro-analytes via $NH_2 \rightarrow Zn^{2+}$ coordination.

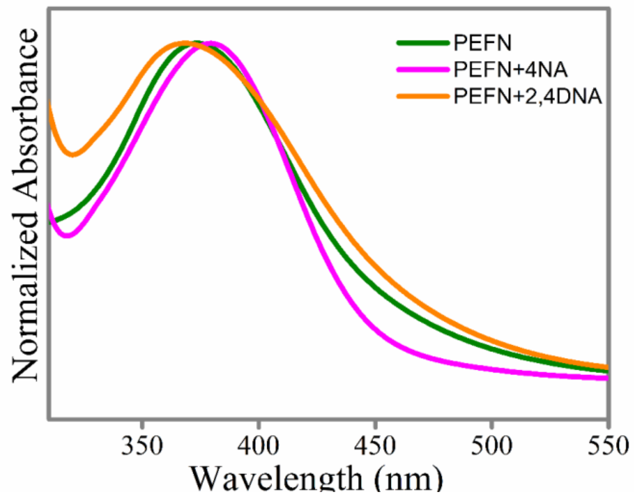

Fig. S14. UV–Vis absorption spectra of PEFN before and after addition of NA and 2,4-DNA, showing shift of the 375 nm band without spectral broadening, consistent with ground-state complex formation and absence of nanoparticle aggregation. UV–visible absorption spectra show distinct shifts in the absorption maxima of PEFN upon interaction with nitroaniline (Fig. S13, ESI), providing further evidence for ground-state complex formation.

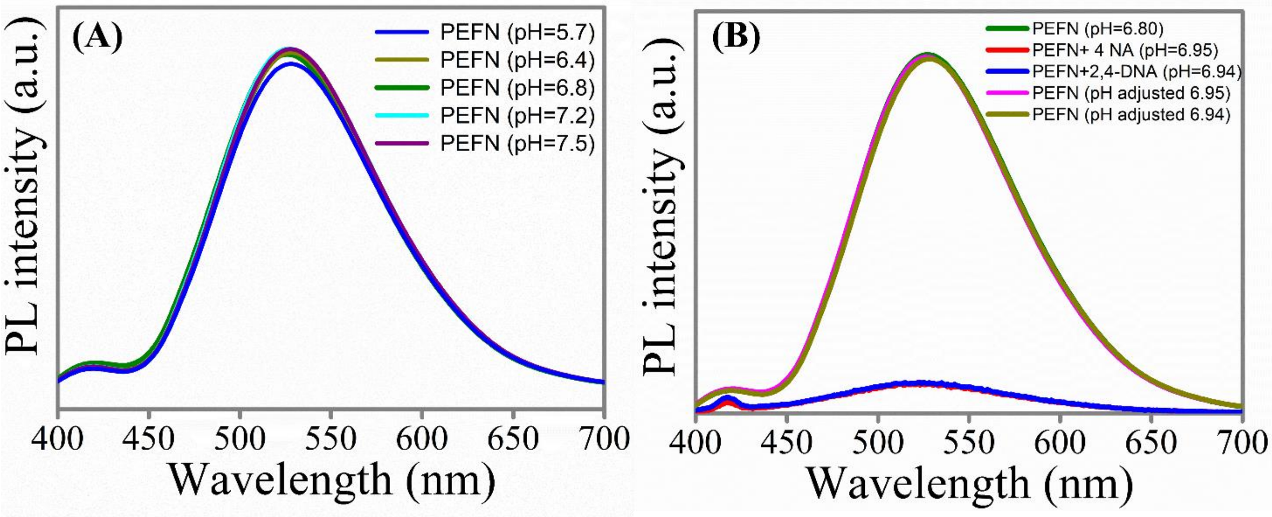

Fig. S15. pH-dependent fluorescence response of PEFN (originally synthesized at pH 6.8). **(A)** Emission intensity across the pH range of 5.7–7.5. **(B)** Fluorescence response upon addition of nitroaniline at the highest analyte concentration within the linear detection range. The results demonstrate pH-independent emission behavior, with PEFN solutions adjusted to the indicated pH values prior to measurement.

Table S1. Fluorescence lifetime parameters of PEFN and ZQC, demonstrating plasmon-enhanced emission lifetime of PEFN relative to ZQC.

Sample	A_1	τ_1 (ns)	A_2	τ_2 (ns)	χ^2	τ_{av} (ns)
PEFN	94.23	3.19	5.78	16.58	1.01	**6.4**
ZQC	37.38	1.18	62.52	3.27	1.07	**2.9**

Table S2. Zeta potential measurements for AgNPs, PEFN, and PEFN complexes with 2,4-DNA and 4-NA. The shifts in zeta potential indicate changes in surface charge associated with the binding of analytes to PEFN.

Samples	Zeta Potential (mV)
AgNPs	-1.26 ± 0.27
PEFN	+0.29 ± 0.04
PEFN +2,4 DNA	-0.85 ± 0.15
PEFN +4 NA	-0.44 ± 0.09

Table S3. Stern–Volmer constants and limits of detection (LOD) for 2,4-DNA and 4-NA determined from fluorescence quenching experiments of PEFN.

Analyte Sample	K_{sv} (M^{-1})	LOD (ppb)	Linear Range (μM)
2,4-DNA	1.6×10^6	1.5±0.1	0.2 - 1.0
4-NA	1.7×10^6	1.4±0.1	0.2 - 1.0

Table S4. Comparison of sensing performance parameters of PEFN with previously reported fluorescent sensors for 2,4-DNA and 4-NA, including LODs and detection ranges.

Ref. No.	Used optical nanoprobe	Detected molecule	LOD
S10	Carbon dots derived from Vitamin B_1	2,4-DNA	0.05 µmol/L
S11	Azine-Triazine-Functionalized CoFs	4-NA	89 ppb
S12	Cd-TEM	4-NA	1.1 ppb
S13	Luminescent Metal-Organic Nanoprobes with Sulfone moiety	4-NA	125 ppb
S14	MoS_2/WC nanocomposite	4-NA	0.034 μM
S15	N-doped Carbon dots with blue and green emission	4-NA	111.6 nM 68.9 nM
S16	Fluorescent anthracene based MoF	2-NA 4-NA 2,4-DNA	0.1033 ppm 0.1026 ppm 0.0997 ppm
S17	Fluorescent molecularly imprinted nanoparticles	4-NA 2,4-DNA	7 nM 6 nM
S18	$BaSnO_3$/HNTs nanocomposites	4-NA	2 nM
S19	Luminescent MoF combining both semi-rigid Tetrapod and rigid Diptotic linkers	4-NA 2,6-DCNA	88 ppb 0.28 ppb
S20	Naphthalene tagged Zn(II) and Cd(II) based luminescent metal–organic probes	4-NA	97 ppb
This Work	PEFN	4-NA 2,4-DNA	1.5 ppb 1.4 ppb

In comparison to previously reported fluorescent probes (Table S4, ESI), PEFN exhibits superior performance in terms of detection limits, response time, selectivity, and aqueous stability.

Table S5. Detection of 2,4-DNA and 4-NA in real water samples using PEFN, showing concentrations, recovery values, and RSDs (n = 3) that demonstrate robust performance in complex matrices.

Analyte	Samples	Spiked (μM)	Calculated (μM)	Recovery ±RSD (%)
2, 4- DNA	River Water	0.208	0.213	103.00 ± 0.48
		0.416	0.453	108.97 ± 1.23
		0.625	0.609	97.49 ± 0.24
	Tap Water	0.208	0.201	96.63 ± 1.73
		0.416	0.406	97.52 ± 1.21
		0.625	0.638	102.13 ± 1.04
4 -NA	River Water	0.208	0.218	104.65 ± 0.73
		0.416	0.417	100.24 ± 1.27
		0.625	0.640	102.40 ± 0.32
	Tap Water	0.208	0.199	95.83 ± 0.99
		0.416	0.405	97.36 ± 0.71
		0.625	0.603	96.59 ± 0.84

Table S6. Fluorescence lifetime parameters of PEFN in the presence of NA and 2,4-DNA, showing negligible changes in decay times and confirming a static quenching mechanism.

Analyte	A_1	τ_1 (ns)	A_2	τ_2 (ns)	χ^2	τ_{av} (ns)
4-NA	93.57	3.59	6.43	15.09	1.10	**6.1**
2,4-DNA	91.92	3.52	8.08	14.21	1.01	**6.3**

References

S1). S. D. Solomon, M. Bahadory, A. V. Jeyarajasingam, S. A. Rutkowsky, C. Boritz and L. Mulfinger, *J. Chem. Educ.* **2007**, 84,

S2).S. Singha, M. Paul, P. Ghosh, M. Manna, S. Pramanik, A. Misra and S. Bhandari, *J. Phys. Chem. Lett.* **2025**, 16, 6066

S3).S. Bhandari, S. Roy, S. Pramanik and A. Chattopadhyay, *Langmuir* **2019**, 35, 14399

S4). A. Manivel and S. Anandan, *Colloids Surf. A: Physicochem. Eng. Aspects* **2012**, *395*, 38.

S5). B. Sureshkumar, Y. Sheena Mary, C. Yohannan Panicker, K. S. Resmi, S. Suma, S. Armaković, S. J. Armaković, C. Van Alsenoy, *J. Mol. Struct.* **2017**, *1145*, 421.

S6). S. Kim, S.-W. Joo, *Vibrational Spectrosc.* **2005**, *39*, 74

S7). D. Sobhana, *Asian J. Chem.* **2007**, *19*, 2667

S8). S. Bhandari, S. Roy, A. Chattopadhyay, *RSC Adv.* **2014**, *4*, 24217.

S9). S. Singha, M. Paul, P. Ghosh, M. Manna, S. Pramanik, A. Misra, S. Bhandari, *J. Phys. Chem. Lett.* **2025**, 16, 6066.

S10). S. Li, Q. Zhou, Z. Li, M. Liu, Y. Li and C. Chen, *Spectrochim. Acta Part A Mol. Biomol. Spectrosc***., 2023**, 286, 122040

S11). P. Das, G. Chakraborty and S. K. Mandal, *ACS Appl. Mater. Interfaces*, **2020**, 12, 10224–10232

S12). R. Zheng, Y. Zhang, G. Bao, P. Wu, W. Wei, X. Yuan, T. Zou, T. Zhang and J. Wang, *ACS Sustainable Chem. Eng.*, **2023**, 11, 9077–9086

S13). A. Chanda and S. K. Mandal, *ACS Appl. Nano Mater***., 2025**, 8, 12784–12798

S14). S. Ganesan, T. Kokulnathan and A. Palaniappan, *ACS Appl. Nano Mater.*, 2025, **8**, 7004–7014

S15). N. Nandi, P. Sarkar and K. Sahu, *ACS Appl. Nano Mater.*, **2021**, 4, 9616–9624.

S16). J.-H. Wang, G.-Y. Li, X.-J. Liu, R. Feng, H.-J. Zhang, S.-Y. Zhang and Y.-H. Zhang, *Inorg. Chim. Acta*, **2018**, 473, 70–74.

S17). A. Elbelazi, F. Canfarotta, J. Czulak, M. J. Whitcombe, S. Piletsky and E. Piletska, *Nano Res.*, **2019**, 12(12), 3044–3050.

S18). T. S. Priya, R. Sasikumar, T.-W. Chen, S.-M. Chen, B. Kim and T. Kokulnathan, *Appl. Clay Sci.*, **2023,** 244, 107103

S19). G. Chakraborty, P. Das and S. K. Mandal, *ACS Appl. Mater. Interfaces*, **2018**, 10, 42406–42416.

S20). A. Chanda and S. K. Mandal, *New J. Chem.*, 2022, **46**, 6068–6077
